Article

DNA Translocation in nm-Thick Silicon Nanopores

Julio A. Rodríguez-Manzo, Matthew Puster, Adrien Nicolaï, Vincent Meunier, and Marija Drndic

ACS Nano, **Just Accepted Manuscript** • Publication Date (Web): 02 Jun 2015

DNA Translocation in nm-Thick Silicon Nanopores

Julio A. Rodríguez-Manzo,[*,†,⊥] *Matthew Puster,*[†,‡,⊥] *Adrien Nicolaï,*[§] *Vincent Meunier,*[§,‖] *and Marija Drndić*[*,†]

† Department of Physics and Astronomy, University of Pennsylvania, Philadelphia, Pennsylvania 19104, United States.

‡ Department of Materials Science and Engineering, University of Pennsylvania, Philadelphia, Pennsylvania 19104, United States.

§ Department of Physics, Applied Physics and Astronomy, Rensselaer Polytechnic Institute, Troy, New York, 12180, United States.

‖ Department of Materials Science and Engineering, Rensselaer Polytechnic Institute, Troy, New York, 12180, United States.

KEYWORDS: Nanopore, amorphous silicon, thin membrane, single-molecule sensor, STEM, EELS, DNA.

Abstract

Solid-state nanopores are single-molecule sensors that detect changes in ionic conductance (ΔG) when individual molecules pass through them. Producing high signal-to-noise ratio for the measurement of molecular structure in applications such as DNA sequencing requires low noise and large ΔG. The latter is achieved by reducing the nanopore diameter and membrane thickness. While the minimum diameter is limited by the molecule size, the membrane thickness is constrained by material properties. We use molecular dynamics simulations to determine the theoretical thickness limit of amorphous Si membranes to be ~ 1 nm, and we designed an electron-irradiation-based thinning method to reach that limit and drill nanopores in the thinned regions. Double-stranded DNA translocations through these nanopores (down to 1.4 nm in thickness and 2.5 nm in diameter) provide the intrinsic ionic conductance detection limit in Si-based nanopores. In this regime, where the access resistance is comparable to the nanopore resistance, we observe the appearance of two conductance levels during molecule translocation. Considering the overall performance of Si-based nanopores, our work highlights their potential as a leading material for sequencing applications.

Interest in solid-state nanopores as single-molecule high-throughput sensors arises from their capacity to conduct ionic currents through membranes in a way similar to protein nanopores.[1] However, in contrast to biological nanopores, solid-state nanopores offer tunable size, high bandwidth operation due to ~ nA variation in measured currents, stability in a wide range of salt concentrations and voltages, and intrinsic compatibility with conventional solid-state device fabrication processes, thereby providing great opportunities for widespread deployment and integration with other technology. This possibility is demonstrated in their coupling with tunneling electrodes,[2] silicon nanowire field-effect transistors,[3] graphene nanoribbons[4,5] and zero-mode waveguides.[6]

Nanopores sense the presence of individual molecules *via* a change in ionic conductance ΔG. Here we use the convention that a positive ΔG represents a drop in conductance, namely $\Delta G = G_0 - G_{with\ molecule}$, where G_0 is the open nanopore conductance and $G_{with\ molecule}$ is the conductance when the nanopore is partially blocked by a translocating molecule (Figure 1a). Hence, the magnitude and statistical properties of ΔG provide good metrics for the nanopore's sensing capability. Increasing ΔG (or ΔI) and decreasing the signal noise, namely the root-mean-square (RMS) deviation of G_0 ($G_{0\ \mathrm{RMS}}$), yield a higher signal-to-noise ratio (SNR) ~ ΔG / $G_{0\ \mathrm{RMS}}$, broadening the frequency bandwidth at which nanopore setups can operate.[7–10] Thus, assuming constant noise, increasing ΔG improves the performance of nanopore sensors. For example, when a nanopore senses molecular translocations with ΔG ~ 10 nS and up to 20 % RMS noise the accessible bandwidth expands to the MHz range.[9] A solid-state nanopore platform with a membrane thickness of four DNA bases (~ 1.3 nm), with sufficiently low noise,[10] and producing discrete signals for all possible combinations of the four DNA bases as in the case of protein nanopores,[11] could conceivably be used to sequence an entire human genome. Therefore, a clear

understanding of what is the practical upper limit to ΔG and which nanopore fabrication procedure, including choice of membrane material, is ideal for attaining the highest ΔG is crucial for the design and fabrication of solid-state nanopore-based sensors.

Maximum ΔG occurs when the molecule completely blocks the ionic current flow through the nanopore (*i.e.*, $G_{with\ molecule} \sim 0$ and $\Delta G \sim G_0$). This condition is satisfied by making the nanopore diameter close to the molecule size in order to maximally block ionic current during molecule transit. Likewise, since ionic resistance is directly proportional to membrane thickness in the limit of negligible access resistance,[12] reducing the thickness increases G_0 when considering the approximation of the nanopore as a cylindrical conductor with a length equal to the membrane thickness.[13] Therefore, maximizing ΔG requires matching the nanopore diameter to the molecule cross-section and minimizing its thickness. Efforts to fabricate thin membranes include thinning silicon nitride (SiN_x) films with reactive-ion etching[14,15] or a focused helium-ion beam[16] and using thin materials such as graphene,[17–20] boron nitride,[21,22] ALD-grown hafnium oxide[23,24] and molybdenum disulfide.[25]

Here we describe a method to thin free-standing SiN_x films to < 2 nm and fabricate nanopores using the electron probe of a scanning transmission electron microscope (STEM) operated at 200 kV, and we show DNA translocations through nanopores with diameters just slightly larger than a double-stranded molecule (diameter ~ 2.2 nm). The electron probe, with a 0.5–2.4 nm diameter, is scanned over a film area while high-angle annular dark-field (HAADF) STEM images and energy electron-loss spectra (EELS) are acquired continuously and simultaneously, as depicted in Figure 1b. Electron irradiation causes sputtering of N and Si atoms,[26] and film thickness is controlled by observing and quantifying this mass loss with the HAADF STEM images and EELS. For a sufficiently large electron dose, defined as the total charge deposited per

unit area, this method produces an amorphous silicon (*a*-Si) membrane owing to the larger sputtering rate of N compared to that of Si.[27,28] This implies that, when compared with a silicon nitride membrane of the same thickness, an *a*-Si membrane is more stable under electron irradiation. In STEM, probe size and lateral movement can be controlled with sub-nanometer precision. This spatial resolution is transferable to the final drilling step that defines nanopore size and position.[4] We also perform large-scale molecular dynamic (MD) simulations that demonstrate that free-standing *a*-Si membranes become unstable for thicknesses ~ 1 nm, indicating that our thinning method produces membranes close to the theoretical stability limit.

Nanopores prepared using the new electron-irradiation-based method developed here show ΔG as high as 9.7 ± 0.4 nS for the translocations of double-stranded DNA (dsDNA) scaled to 1 M KCl electrolyte solution at room temperature (23°C). This corresponds to a mean percentage of ionic conductance blocked during translocation (% of ΔG / G_0) reaching values up to 85 % in 2.5-nm-diameter nanopores. The associated SNR presents values up to ~ 70 at 100 kHz for our measured ionic current RMS noise ~ 80 pA at 500 mV ($G_{0\ \mathrm{RMS}}$ ~ 0.16 nS). We contrast these results with recent reports describing translocations of DNA through nanopores drilled in membranes of different materials with thicknesses < 10 nm.[14,17–23,25,29,30] In particular, our comparative study shows that the ΔG data reported here are within experimental error bar of the best measurements of dsDNA translocations through any solid-state nanopore measured in KCl solution that are dominated by SiN_x nanopores. Moreover, our highest ΔG surpass all but one data point (Table 1) measured on nanopores in 2D materials (graphene, MoS_2 and BN), as small-diameter nanopores in these materials have not been realized yet.

Our findings on the development of a method to thin *a*-Si membranes down to 1.4 nm, close to the theoretically determined thickness limit of ~ 1 nm, and on the determination of the ionic

conductance upper limit for translocation of DNA through Si-based nanopores constitute a new technological frontier for solid-state-nanopore based detection. Our research establishes that the thinnest Si-based nanopores consistently offer the highest signals (~ 10 nS for dsDNA at 1 M KCl at 23°C) and SNR (~ 70 at 100 kHz, even without optimizing the chip capacitance[10]), well above data reported for any 2D material.

Results

We first illustrate the electron-irradiation-based method by showing results obtained from the thinning of a 50-nm-thick Si_3N_4 film, as captured by HAADF (Figure 1c) and EELS (Figure 1d) signals. A 2.4-nm-diameter probe with current density of 4.8×10^9 A m^{-2} was scanned continuously over a 256 × 256 grid covering a 63 × 63 nm^2 surface until all material was sputtered. The intensities of HAADF and EELS signals are proportional to the number of atoms interacting with the electron probe for film thicknesses less than the scattered electron's mean free path, which is > 100 nm for 200 keV electrons scattered elastically or inelastically in *a*-Si.[31] Therefore, the HAADF and EELS signals from elastically and inelastically scattered electrons provide real-time feedback of the thinning. As the film is thinned with the probe the EELS signal drops, the Si *L*-shell ionization edge maximum exhibits a downward shift of 5 eV and the N *K*-edge fades, indicating loss of mass and N depletion.[27,28] The EELS Si and N ionization edge signals scaled to highest magnitude as a function of electron dose, shown in Figure 1e, prove that a 50-nm-thick Si_3N_4 film thinned with the above irradiation parameters experiences a > 90 % drop in N content with respect to Si for an electron dose of 4×10^9 C m^{-2}. Hereafter, we refer to those membranes exhibiting atomic ratios N:Si < 0.1 as "*a*-Si membranes". For the thinnest

membranes the EELS N *K*-edge was indistinguishable from background noise. Milder irradiation conditions (for example, 1.6-nm-diameter probe with current density of 0.4×10^9 A m^{-2}) were necessary during the final thinning step to keep the sputtering rate low (~ 1 nm per minute). This is shown in Figure 1f, where HAADF and EELS signals corresponding to 3.5 and 1.6 nm (± 5 % error) were recorded during the thinning of a 5-nm-thick *a*-Si membrane before the membrane failed. The thinnest membrane measured here had a thickness of 1.4 ± 0.1 nm.

MD simulations of *a*-Si membranes of thicknesses ranging from 0.5 to 5.0 nm establish the theoretical minimum thickness to be ~ 1 nm. Results shown here were obtained from a 8.69 × 8.69 nm^2 cell periodically reproduced in both lateral dimensions (see Methods for details). First, we calculated the surface energy of the membranes as a function of thickness t (Figure 2a). Starting from 5 nm, the surface energy increases quasi-linearly down to t = 1.5 nm. At this point, the surface energy drops to a minimum for t = 0.7 nm, reaching a surface energy as low as that of a 10-nm-thick film. For *a*-Si membranes thinner than 0.7 nm the surface energy increases sharply, indicating the difficulty of further thinning, based on thermodynamic stability arguments alone. Below 0.7 nm, *a*-Si membranes are too thin to sustain bulk-like atoms and consist only of surface atoms. This is shown in Figure 2b, where we plot the density of Si atoms along the normal direction of the membrane. Only two well-defined peaks are present for t = 0.5 and 0.6 nm, whereas the density shows three well-defined peaks for t > 0.7 nm. These three peaks are related to the two surfaces and one bulk-like layer stabilizing the membrane. A thickness of 0.7 nm represents the physical crossover point below which a bulk-like layer is unsustainable.

We gain further insight into the stability of the thinnest *a*-Si membranes by examining their average atomic connectivity (Figure 2c). The membranes become unstable when there is a large change in atomic connectivity since this indicates a significant reduction in chemical binding.

The decrease in connectivity is slow until $t = 1.0$ nm, but experiences a large decrease for $t < 1.0$ nm, further indicating that the smallest achievable thickness is in the vicinity of this value. The thermodynamic arguments presented thus far indicate that *a*-Si membranes are unstable below 0.7–1.0 nm, depending on whether we use surface energy or chemical connectivity as metrics for stability. We can further narrow down this range by examining energy fluctuations as a measure of dynamical stability. During MD relaxation, one observes large variations in energetics and structural deformation of *a*-Si films for $t < 1.0$ nm, as quantified by the root-mean-square deviation (RMSD) of atomic positions, which captures the structural fluctuations and the variance of the energy during MD simulations (Figure 2d). These two metrics of fluctuations increase rapidly for thicknesses < 1.0 nm, indicating the difficulty of creating a stable *a*-Si membrane with $t < 1.0$ nm and supporting the experimental evidence that the thickness limit lies at ~ 1 nm.

Once the film is thinned, the final step required to make a nanopore involves acquiring a STEM HAADF image of the membrane and positioning the electron probe on a chosen pixel until the drop in EELS signal indicates that all material inside the probe (~ 10^3 Si atoms) has been sputtered (Figure 3a). Nanopores were made with probe diameters of 1.3–2.4 nm with a current density of 0.3×10^9 A m^{-2}. For membranes with thicknesses < 10 nm, nanopores are made in a few seconds with these conditions, with diameters a few angstroms wider than the probe. The probe size and convergence angle, together with the electron dose, provide a wide palette of settings to make nanopores of different sizes with sub-nanometer precision (Figures 3b). When the nanopore axis is tilted with respect to the electron beam, a transmission electron microscopy (TEM) image displays the projection of the nanopore shape (Figure 3c). For thick membranes (for example, 100 nm), these drilling conditions generate a nanopore with a

truncated cone shape, and for membranes < 10 nm thick, the nanopore shape becomes indistinguishable from that of a cylinder. At this level, for example, less than 10 Si atoms span the length of a 2-nm-thick nanopore. A typical nanopore fabricated this way is modeled in Figure 3d, showing its scale with respect to a dsDNA molecule in solution. The thinnest STEM-drilled nanopores shown here have a cylindrical shape in contrast to the TEM-drilled pores shown by previous work to have an hourglass shape with effective thickness equal to one-third of the membrane thickness[14]. This would imply that a 1.7–2 nm-thick nanopore drilled by STEM gives comparable ΔG to a 5–6 nm-thick TEM drilled pore.[14,15] In the limit of very thin nanopores approaching two-dimensions, there should be no difference in signal levels between the two cases. Once the *a*-Si nanopores are outside of the TEM vacuum chamber, Si is expected to react with oxygen and form a native oxide layer. It is therefore likely that the nanopores consist of Si encapsulated by SiO_2. We took TEM images of the same nanopore immediately after drilling in vacuum, and then after piranha treatment and air exposure for about one week (Supporting information SI-6). There was not a noticeable change in nanopore diameter.

To assess the ΔG obtained from nanopores made in thinned *a*-Si membranes we measured translocation dynamics of dsDNA (15 kbp and 400 bp) in buffered 1 M KCl solution as a standard molecule to allow for comparison with published literature. We present data from twelve nanopores in *a*-Si membranes, with 2.5–5.3 nm diameters and thicknesses < 10 nm, of which ten had thicknesses ≤ 4 nm and four had thicknesses ≤ 2 nm. TEM images of three individual nanopores are shown in Figures 4a-c, along with a representative 12 second long raw trace of ionic current measured during DNA translocations, and a zoom-in of individual translocation events at shorter time-scales. The single-point-per-event scatter plots show the distribution of events in translocation duration along with the % of ΔG / G_0 and its corresponding

histogram. These events show a ΔG as high as 10.8 ± 0.4 nS for measured conductivity of 12.0 S m^{-1}, corresponding to a solution concentration of 1.1 M KCl at 23°C (or ΔG = 9.7 ± 0.4 nS when scaled to 1 M KCl at 23°C). We did not observe a dependence of ΔG on the applied voltage up to 500 mV, which implies that data acquired at different voltages can be directly compared (Figures 4d-e). For all measurements, nanopore diameters were estimated from TEM images (d_{TEM}), and for the thinnest membranes we also calibrated the membrane thickness from EELS (t_{EELS}). In lieu of an EELS-based estimate of membrane thickness, we used the measured G_0 and ΔG to extract an effective membrane thickness estimate (t_{eff}), as shown in Figure 5a and Supporting Information SI-1, using a cylindrical model for nanopore conductance.[13] Nanopore dimensions and DNA translocation results for all measured nanopores are given in Supporting Table ST-1.

Upon closer inspection of translocation events at short time-scales, it is clear that a significant number of events contain two distinct levels, indicated by green and blue dashed lines in Figure 4e, similar to recent reports.[9,29,32] The advent of the shallow level (ΔG_s) corresponds in our experiments with the regime of nanopores with diameters d < 5 nm in membranes with thicknesses t < 10 nm. In this regime, the nanopore access resistance[12] $(1 /(2 \sigma d))$, where σ is the electrolyte conductivity, is comparable to the resistance of the nanopore itself. Within a single translocation event, a shallow level can appear before or after the deep level, and typically less than one third of events contain a single shallow level without a second deeper level. Typically over 50 % of events contain two levels; although in some instances it is much higher. The smaller % of ΔG / G_0 peak in each scatter plot (Figure 4 a-c) records when the single translocation event consists only of the shallow level. These shallow single-level events have shorter time duration than two-level translocation events. For voltages < 200 mV, there are

practically no deep events, and the only events are shallow single-level events. This event structure occurs in nanopores with diameters down to 2.5 nm, which are not wide enough to allow translocation of DNA in a folded configuration, and for DNA lengths of 15 kbp (Figure 4) and 400 bp (Supporting Information SI-2). It has been proposed that the shallow level is related to the presence of the molecule in the access region of the nanopore.[29] ΔG of the deep level scales with membrane thickness, indicating that that level represents full molecular translocation,[14] while the magnitude of the shallow level ΔG_s is not dependent on membrane thickness (Figure 5b) In the previous work by Carlsen *et al.*[29] on 4.5-nm-thick SiN_x nanopores, the shallow level was observed before the deep level and was attributed to the current blockade before the DNA molecule enters the nanopore. However, we also observe events when the shallow level occurs after the deep level, which may be attributed to the DNA molecule exiting the nanopore. We note that the nanopores studied here are significantly thinner than those used by Carlsen *et al.*,[29] which may be the reason why we may observe the exit of the molecule. Further translocation measurements will need to clarify this point.

As the nanopore diameter is decreased down to the dsDNA diameter, the noise in ionic conductance during translocation (ΔG_{RMS}) becomes larger than $G_{0\ RMS}$, and the duration of the events increases up to two orders of magnitude (Figure 4 a-c). For measurements of dsDNA through nanopores narrower than 2.5 ± 0.2 nm in diameter, nanopore clogging occurs quickly. The % of ΔG / G_0 plateaus at 85 % for dsDNA translocations through nanopores down to 2.5 nm in diameter (Figure 5c).

The nanopores are stable in ionic solution and can probably last for hours. Most of our translocation measurements lasted around 10 minutes (yielding thousands of translocation events) and we have not studied how long they can ultimately last. The main challenge includes

possible nanopore expansion in time, shifting the open-nanopore current baseline, G_0. Further systematic studies of nanopore durability as a function of applied voltage, salt concentration and other external conditions are required before implementing these nanopores into any future sequencing platforms.

At this stage in the ten-year-long development of the solid-state nanopore field, it is important to compare quantitatively between the best ΔG for DNA reported in the literature in order to rationalize the optimal choice of membrane materials and nanopore dimensions moving forward, Table 1 ranks results collected across the literature according to ΔG, for nanopores made in membranes with thicknesses < 10 nm, together with the highest ΔG for dsDNA obtained in this work. Four out of the top six results from Table 1, including ours, were measured with Si-based nanopores. The electrolyte conductivity was not measured in all published studies. In these cases, we assumed standard values (Supporting Information SI-3). It is important to note that ionic current data is exceptionally sensitive to the electrolyte conductivity. An increase in temperature of 5ºC can give a 10 % change in conductivity for the same nanopore diameter and thickness. Similarly, a 0.2 M increase in KCl concentration produces an error in conductivity that can yield an 18 % change in ΔG.

The trends in ΔG based on material choice, membrane thickness, and nanopore diameter become even more evident in Figure 5d, where ΔG is plotted with respect to the corresponding G_0 for all compiled data from the literature for dsDNA translocations through nanopores < 10 nm thick. Data was scaled to an electrolyte conductivity of 10.8 S m^{-1}, representing 1 M KCl at 23°C. ΔG and G_0 are the directly measured experimental quantities, and this allows a comparison of published results without any fitting for membrane thickness or nanopore diameter, keeping in mind that error bars for published results where electrolyte conductivity was not measured may

be large. The upper limit of 100 % conductance blocked ($\Delta G_{max} = G_0$) is indicated by a straight dashed line in Figure 5d. To achieve a higher ΔG, one may move up the $\Delta G = G_0$ line by decreasing the membrane thickness for a constant nanopore diameter, which increases both G_0 and ΔG. At the limit of vanishing thickness, the resistance is determined by the access resistance alone for a given nanopore size, and any subsequent increase in G_0 can only be achieved by an increase in diameter. When the diameter increases, however, ΔG begins to decrease. Conceptually, this should result in a maximum peak in ΔG as a function of G_0, and in fact that trend proves to be experimentally true (Figure 5d). To visualize this trend dashed lines of either constant membrane thickness or constant nanopore diameter portray the dependence of ΔG on G_0, based on the cylindrical model referenced before. Instead of a sharp peak, as predicted by that model, there appears to be a rounded maximum. To achieve the maximum ΔG both the membrane thickness and nanopore diameter must be small. Thus, although according to their thicknesses nanopores made in 2D materials should yield the highest ΔG, the majority of reported results for 2D materials fall short of the ΔG values reported for Si-based nanopores. All the data in Fig. 5d except for one point fall within the range on the plot bounded by the ΔG isoline for t = 1 nm and $\Delta G = G_0$. The point by Carlsen *et al.*[29] seems to be an outliner on this graph. This could happen if there were any discrepancies between the nominal solution concentration reported (0.9 M NaCl) and the actual solution concentration (and conductivity). Another potential reason could originate from differences in translocation dynamics in NaCl *vs.* KCl that may not allow a simple linear scaling of ΔG.

Conclusions

In summary, the electron-irradiation-based thinning method outlined here can be consistently employed to fabricate *a*-Si nanopores < 2-nm-thick with diameters tailored to molecule size with sub-nanometer precision. We used this method to reach the theoretical thickness limit of *a*-Si membranes, which we established to be ~ 1 nm with MD simulations and corresponds to about 3–4 DNA bases. Double-stranded DNA translocation measurements with these nanopores at the thickness limit provide the intrinsic ionic conductance detection limit in Si-based nanopores (*i.e.*, ~ 10 nS at 1 M KCl at 23°C for dsDNA) and show a two-level event structure. Our work establishes that compared with other materials, Si-based nanopores remain unrivaled in terms of ease of fabrication, robustness to chemical treatments and applied bias, wettability, ionic current noise, and yield.

Methods

Free-standing 50 × 50 μm^2 Si_3N_4 films supported on 5 μm SiO_2/500 μm Si wafers were fabricated with standard lithographic procedures.[14,15] The 5-nm-thick *a*-Si film used in Figure 1f was purchased from SIMPore Inc. STEM and TEM were carried out with a JEOL 2010F operating at 200 kV. The HAADF signal was collected from electrons scattered at angles > 50 mrad. The current density of the electron probe (0.3–4.8 × 10^9 A m^{-2}) was modified by changing the probe size or/and varying its convergence angle. Quoted probe diameters (0.5–2.4 nm) correspond to the manufacturer specifications. Typically STEM conditions for thinning were: pixel size of 0.16–0.33 nm and dwell time of 20–160 μs. EELS was acquired with a GIF camera (Gatan Inc.) with dispersion of 0.5 eV/channel and convergence collection angle of 15 mrads.

During thinning EELS spectra were acquired every 0.01 seconds. Quantification of the N and S ionization edges was performed with CSI spectrum analyzer.[33] We prepared KCl solutions with 10mM tris and 1mM EDTA. Solution conductivities and temperatures were measured with an Accumet pH/conductivity meter. We obtained conductivities between 12.0 and 12.2 S m^{-1} which correspond with approximately 1.1 M KCl. 15kbp and 400bp dsDNA fragments were purchased from Fermentas Life Sciences. Typically we used 40 ng of DNA per μL of KCl solution. Ionic current data was acquired with a patch-clamp amplifier (HEKA Elektronik Dr. Schulze GmbH), sampled at 200 kHz, and filtered at 100 kHz; except for events collected at 100 mV, which were filtered at 10 kHz. The nanopore chip was cleaned using hot piranha solution (i.e., a mixture of sulfuric acid and hydrogen peroxide used to clean organic residues) followed by repeated water rinsing. Translocation events obtained at 500 mV were defined as changes in the open nanopore current > 1 nA concomitant with translocation times > 20 μs. Small modifications to these parameters did not significantly affect the results of the analysis. More details of the statistical analysis of the translocation events are given in Supporting Information SI-4. Generation of computational models of *a*-Si bulk and membranes: we used the LAMMPS software package for all MD simulations.[34] To create *a*-Si bulk material, we employed the method of "melting and quenching". The detailed protocol to fabricate atomic-scale structural models of *a*-Si has been described in detail before.[35] A cubic cell of a = 8.69 nm with periodic boundary conditions and containing 32768 Si atoms was employed to build a three-dimensional bulk unit cell. The Si atoms interactions are modeled using a specific parameterization of the Stillinger-Weber potential.[36] The density of the MD cell was chosen as the same as of crystalline Si (*c*-Si). The atoms were initially arranged in the diamond structure. The amorphous structure was obtained by, first, equilibrating the system at T =3500 K during 100 ps and then quenching it to T = 500 K

during 3 ns. Then, the structural properties of the corresponding *a*-Si bulk material have been compared with experimental data (Supporting Information SI-5). Theoretical and experimental radial distribution functions were found to be in good agreement. The angular distribution of the bonds between first neighbors, with a mean angle of the distribution equal to 109.6° and the standard deviation is equal to 9.5°, are in good agreement with previous works.[37,38] We created the *a*-Si nanoporous membranes from the realistic model for bulk *a*-Si. A film of thickness t is extracted from *a*-Si bulk material by removing all the atoms i of the bulk such as $z_0 - h / 2 > z(i) > z_0 + h / 2$ where z_0 is the median plane of the simulation box used for *a*-Si bulk. Each *a*-Si film is then relaxed at $T = 300$ K during 1 ns.

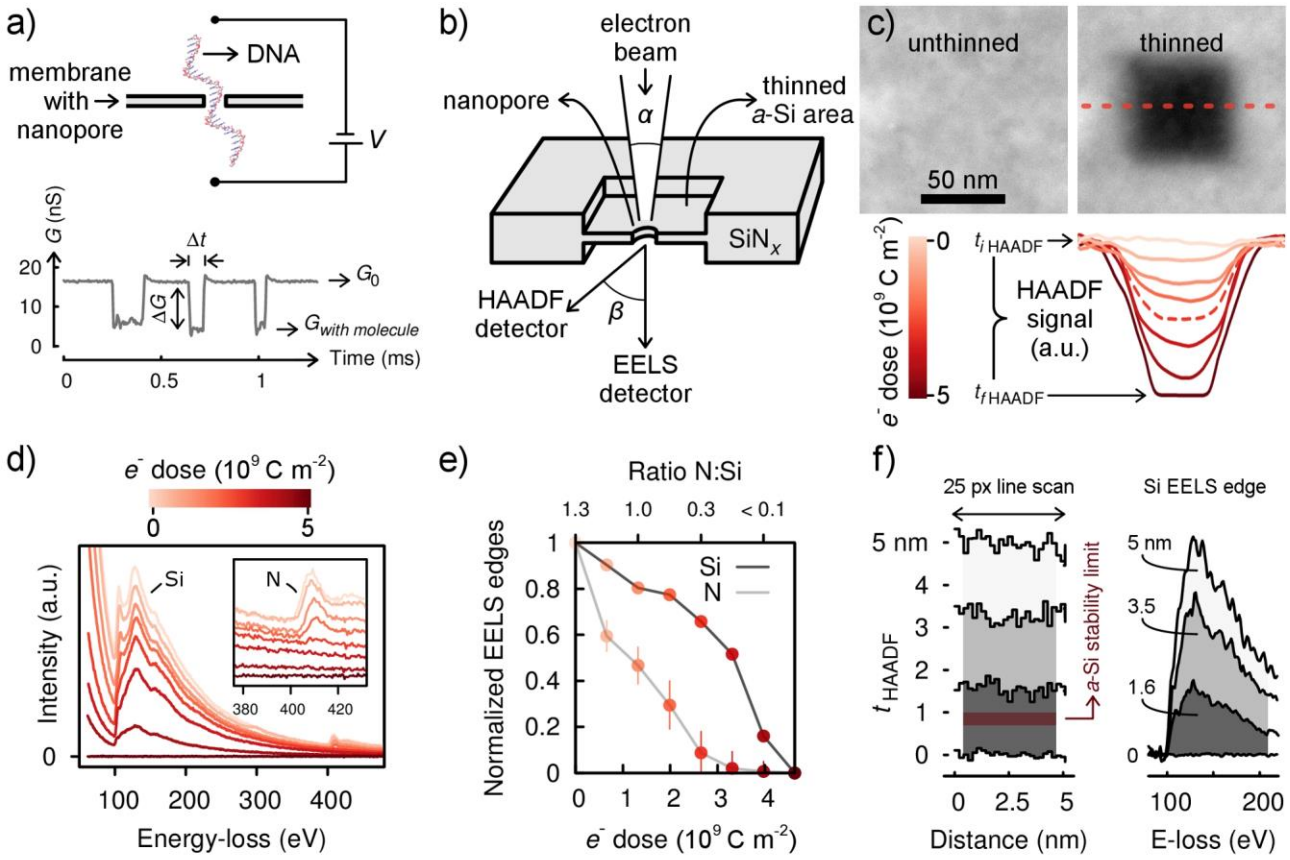

Figure 1. Electron-irradiation-based thinning of Si-based films for nanopore sensors. a) Schematic of DNA translocating through a nanopore and experimental ionic conductance trace showing three concatenated DNA translocations. Each DNA translocation is registered as a change in ionic conductance, $\Delta G = G_0 - G_{with\ molecule}$, and has a translocation time Δt. b) Diagram of electron-irradiation-based thinning method. After interacting with the film the electron beam is collected with HAADF and EELS signal detectors. c) HAADF STEM images of a Si_3N_4 area before (left) and after (right) thinning. Line profiles, as the one indicated by the dashed line, acquired at eight different electron (e^-) doses show an HAADF signal drop with thinning. HAADF signals corresponding to the initial (50 nm) and final (0 nm) thicknesses are indicated by $t_{i\ \mathrm{HAADF}}$ and $t_{f\ \mathrm{HAADF}}$, respectively. d) EELS taken from the SiN_x areas irradiated with electron doses displayed in (c). The Si *L*-edge maximum shifts from 106 to 101 eV with thinning. Onset

of the Si *L* and N *K*-edges corresponds to 100 and 400 eV, respectively, in the EELS signal.[31] e) Si *L* (dark gray) and N *K*-edge (light gray) EELS signals shown in (d) normalized by highest magnitude as a function of electron dose. The top axis indicates the ratio of N to Si atoms. f) HAADF signal (left) and EELS Si *L*-edge (right) corresponding to the thinning of a 5-nm-thick *a*-Si membrane to 3.5 and 1.6 nm. The HAADF signal corresponds to a line scan of 25 pixels and the EELS signal was averaged over 160 pixels of the scan. The *a*-Si theoretical thickness limit (0.7−1.0 nm) is indicated by a red band in the HAADF signal.

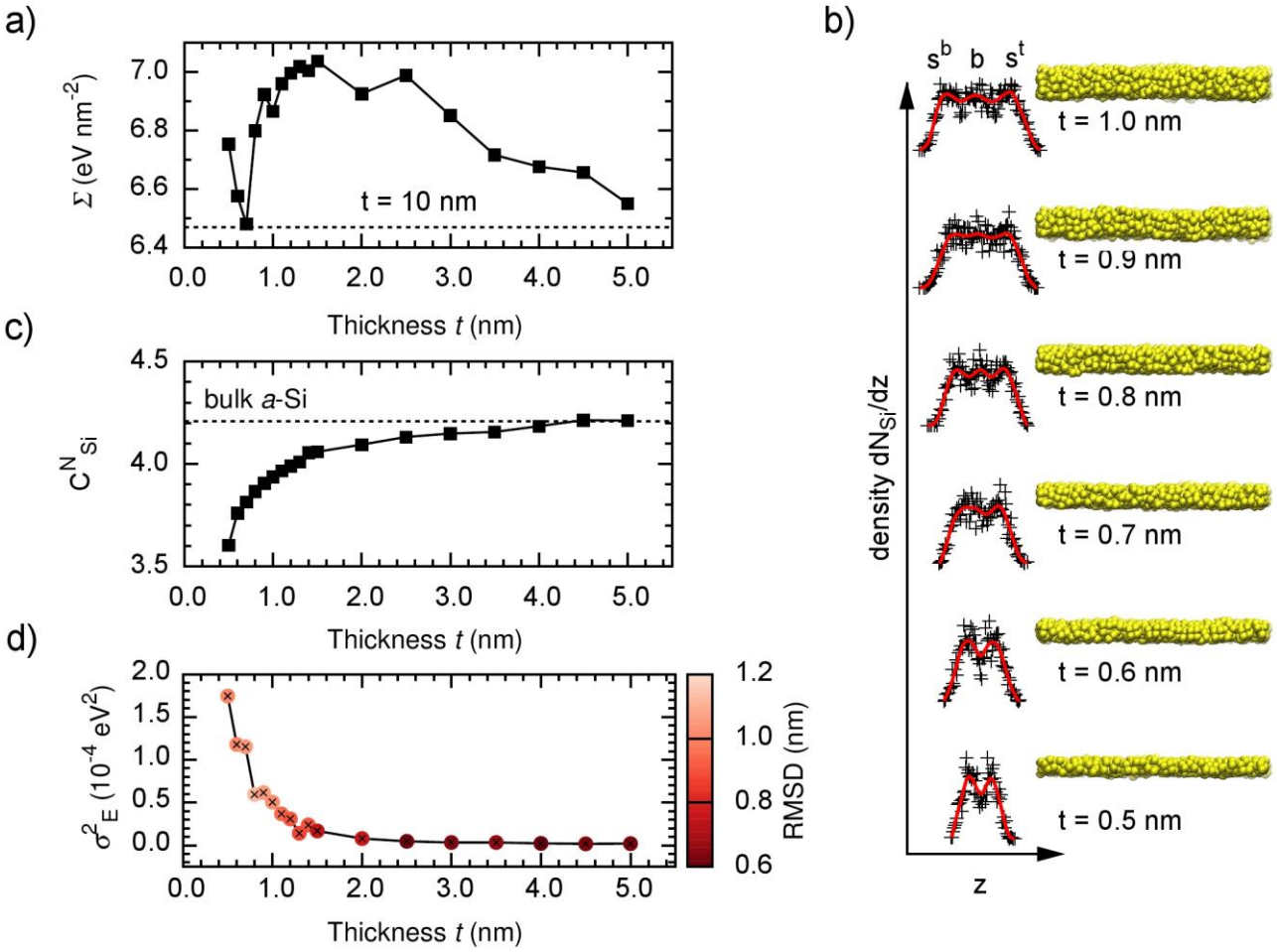

Figure 2. Molecular dynamic simulations and stability analysis of *a*-Si membranes. a) Surface energy Σ as a function of *a*-Si membrane thickness. The dashed line indicates the Σ for a 10-nm-thick *a*-Si film. b) Density of Si atoms dN_{Si} / d*z* along the normal direction *z* perpendicular to the surfaces for *a*-Si films with thicknesses t = 0.5, 0.6, 0.7, 0.8, 0.9 and 1.0 nm. The dN_{Si} / d*z* values smoothed using Bézier curves are shown with red lines. The outermost peaks correspond to the surface atoms. Labels s_b and s_t refer to the bottom and top surfaces, respectively, and *b* to bulk-like atoms. Atomic models for each thickness, represented by spheres with van der Waals radius, are shown on the right. c) Average number of bonds per Si atom C^N_{Si}, computed as the average number of Si atoms in a 0.3 nm diameter sphere centered on each atom, as a function of *a*-Si membrane thickness. The dashed line indicates the C^N_{Si} for bulk *a*-Si. d) Variance σ^2_E of the

energy per Si atom and Si atom distance root-mean-square deviation (RMSD) of Si atomic positions computed during the 1 ns MD relaxation of *a*-Si films as a function of *a*-Si film thickness; σ^2_E represents the amplitude of energy fluctuations at room temperature and measures the structural stability.

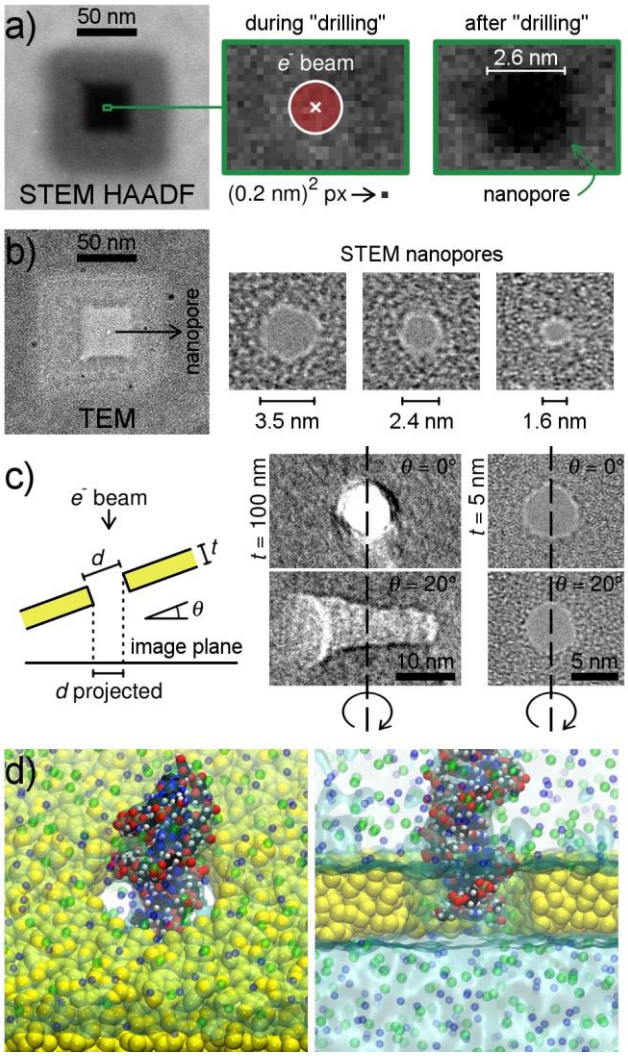

Figure 3. Fabrication and characterization of nanopores in thinned *a*-Si membranes. a) Nanopore "drilling" step. The STEM HAADF image shows a typical two-step thinning formed by a coarse thinning (110 × 110 nm^2) followed by a milder thinning (40 × 40 nm^2). The magnified view of the green rectangle (middle panel) shows how the electron probe is positioned in a selected pixel (0.2 × 0.2 nm^2) during "drilling". The rightmost panel shows a STEM HAADF taken immediately after the nanopore was formed. b) TEM images showing an *a*-Si thinned membrane with a nanopore, and three nanopores (diameters 3.5, 2.4, and 1.6 nm) made in STEM mode with different probe conditions. c) The diagram depicts the projection of a nanopore shape, with diameter *d* and thickness *t*, in the TEM image plane when the nanopore axis is tilted by an angle

θ with respect to the electron beam axis. Nanopores formed in 100- and 5-nm-thick SiN_x membranes are shown at 0 and 20 degrees tilt angle. The dashed line indicates the rotation axis. For the 5-nm-thick membrane, the projected nanopore looks the same as the non-tilted image, which implies a cylindrical shape. d) Top and side views of a snapshot showing realistic molecular dynamics modeling results of a dsDNA molecule translocating across a 2-nm-thick *a*-Si nanopore with 2.7 nm diameter. The simulation involves dynamics where all atoms were treated explicitly, including Si (yellow), water (shown here as a blue hallow), dsDNA, and the positive (blue) and negative (green) ions.

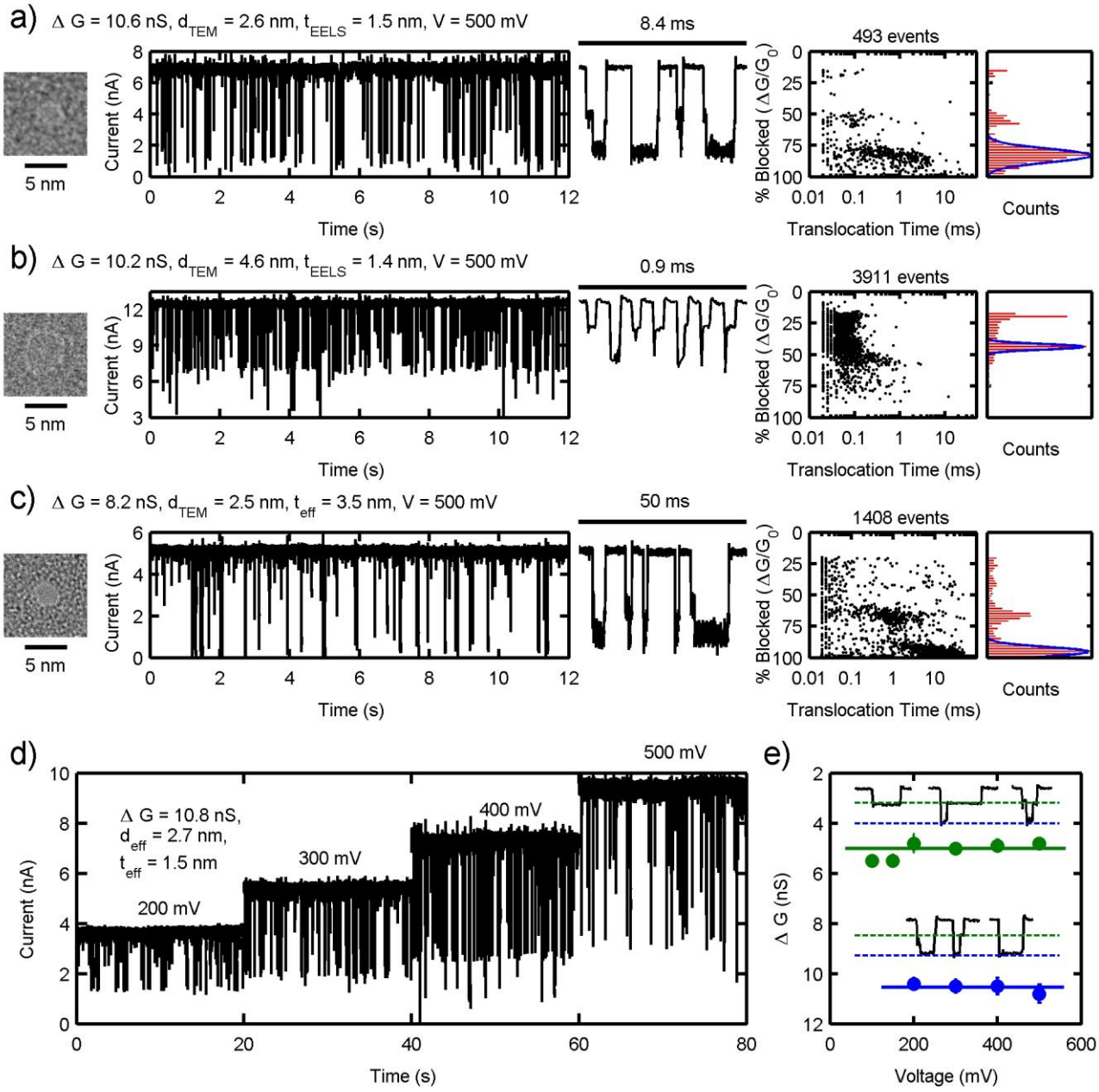

Figure 4. Measurements of dsDNA translocations through nanopores in thinned *a*-Si membranes. a-c) Data from three nanopores with dimensions indicated. From left to right: i) TEM images, ii) ionic current time traces showing 15 kbp dsDNA translocations, iii) representative concatenated events shown at shorter time-scales with the same y-axes scale as (ii), iv) single-point-per-event scatter plots showing event distributions in % of ΔG / G_0 and translocation time, and v) histograms of events for % of ΔG / G_0 with gaussian fit of the primary

translocation peak. TEM images were taken with a low electron dose and resolution to avoid altering nanopore size. All data sets were measured at 500 mV in KCl solution. The solution conductivity and temperature were measured before each experiment and are provided in the table of SI-1. d) Ionic current translocation time traces measured for several voltages from the same nanopore. e) The blue points show ΔG for each voltage shown in (d), and the green points represent the shallow ΔG_s level. Neither the shallow level, nor the full-translocation level exhibit voltage-dependence, emphasized with solid trend lines. Inset shows six representative translocations at 300 mV that demonstrate the structure of the two levels (also seen in a-c). Dashed lines depict where the shallow and full levels lie on the translocations.

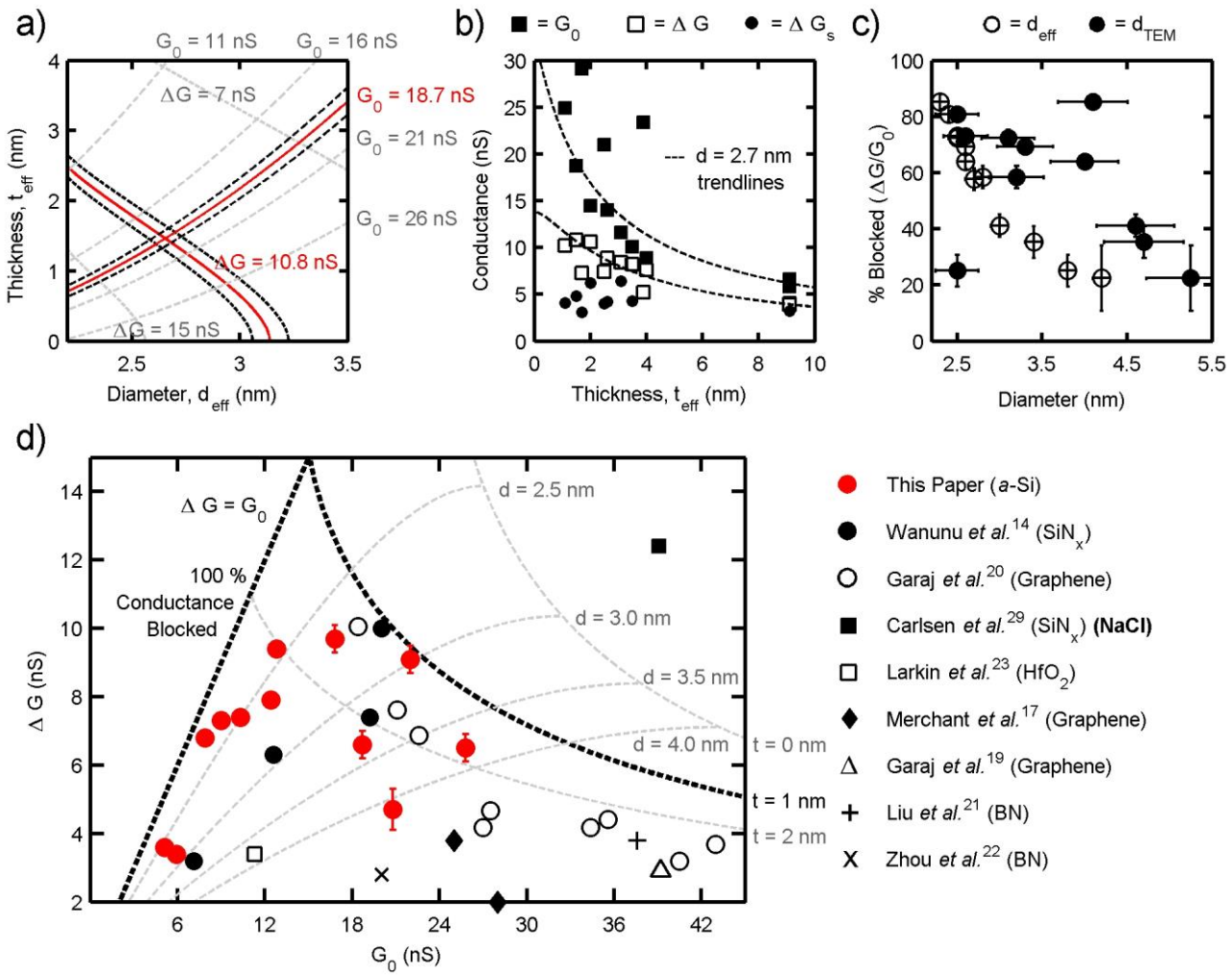

Figure 5. Conductance results from *a*-Si nanopores as a function of nanopore diameter and thickness and comparison with sub-10 nm thick solid-state nanopores in the literature. a) Method of determining d_{eff} and t_{eff} for each nanopore when direct TEM measurements were unavailable. Isolines for the experimentally measured G_0 and ΔG values as a function of nanopore diameter and membrane thickness (red lines with error designated as black dashed lines), according to a cylindrical nanopore model. The intersection of these two isolines gives a solution for d_{eff} and t_{eff} (see Supporting Information SI-1). When effective nanopore dimensions are listed, we have indicated that explicitly. b) G_0, ΔG and ΔG_s values plotted as a function of t_{eff} for all measurements for $t_{\text{eff}} < 10$nm. Nanopore diameters range from $d_{\text{TEM}} = 2.5$ nm to 5.3 nm, and the

dashed lines are trend lines for d = 2.7 nm (Supporting Information SI-1). c) The % of ΔG / G_0 plotted as a function of nanopore diameter, where open circles are deff and filled circles are d_{TEM}. d) Translocation results from our own experiments plotted along with data from the literature for dsDNA (all data is scaled to 1 M KCl, 23ºC). All measurements were in KCl electrolyte unless otherwise noted. Points close to the $\Delta G = G_0$ line have nanopore diameters close to the size of the molecule. For larger nanopore diameters, the maximum ΔG is limited by the membrane thickness, with thicker membranes giving smaller ΔG values. Isolines for t = 0, 1, and 2 nm are shown as guides for the eye (Supporting Information SI-1). Any data from Table 1 not represented in this graph falls outside the bounds of the graph, with either $\Delta G < 2$nS, $G_0 > 45$ nS, or both, or was obtained for ssDNA. Errors are listed in Supplementary Table ST-1 and appear in each graph when they are larger than the data point markers.

Reference	Membrane material	t (nm)	d (nm)	DNA	Electrolyte solution	σ (S m^{-1})	V (V)	ΔI (nA)	ΔG (nS)	ΔG (nS) scaled to 1 M KCl @ 23°C (σ = 10.8 S m^{-1})	ΔG / ($\sigma \times d_{DNA}$) (dimensionless)
Carlsen *et al.*[29]	SiN_x	1.5*	3.4	ds 3 kbp	0.9 M NaCl	7.6†	0.4	3.5	8.7	12.4	0.52
Larkin *et al.*[23]	HfO_2	2*	1.7*	ss 89 b	1 M KCl	9.6 (25°C)	0.4	1.9	4.7	5.3	0.44
Garaj *et al.*[20]	Graphene	0.6*	2.8	ds 10 kbp	3 M KCl	27.5	0.16	4.1	25.6	10.1	0.42
Wanunu *et al.*[14]	SiN_x	2.6*	4	ds 3 kbp	1 M KCl	13.7 (21°C)	0.3	3.8	12.7	10.0	0.42
This work	*a*-Si	1.5	2.7*	ds 15 kbp	1.1 M KCl	12.0	0.5	5.4	10.8	9.7	0.41
Yanagi *et al.*[30]	SiN_x	3.7*	2.3*	ss 5.3 kb	1 M KCl	10.5 (22.5°C)	0.3	1.4	4.7	4.8	0.40
Merchant *et al.*[17]	Graphene / TiO_2	6 –10	5 × 7	ds 400 bp	1 M KCl	10.8†	0.15	1.1	7.3	7.3	0.31
Liu *et al.*[21]	BN	1.1	5 × 6	ds 10 kbp	3 M KCl	28.7†	0.16	1.6	10.0	3.8	0.16
Zhou *et al.*[22]	BN	–	4	ds 48 kbp	1 M KCl	10.8†	0.15	0.4	2.8	2.8	0.12
Garaj *et al.*[19]	Graphene	0.6*	4.6*	ds 10 kbp	3 M KCl	28.9† (24°C)	0.16	1.2	7.8	2.9	0.12
Liu *et al.*[25]	MoS_2	1.6*	20	ds 48 kbp	2 M KCl	20.0 (20°C)	0.2	1.0	5.0	2.7	0.11
Schneider *et al.*[18]	Graphene	0.3	22	ds 48 kbp	1 M KCl	10.8†	0.2	0.3	1.5	1.5	0.06

t: membrane thickness. d: nanopore diameter. σ: electrolyte conductivity. V: applied voltage. ΔI: change in nanopore ionic current. ΔG: change in nanopore ionic conductance.

Table 1: Change in ionic conductance caused by translocating DNA through nanopores fabricated in solid-state membranes with thicknesses < 10 nm. Only the maximum ΔG is quoted for each reference. The data shown in columns 2 through 10 were extracted directly from the literature. Next to last column scales all ΔG to values of 1 M KCl electrolyte at room temperature ((ΔG / σ_{given}) × $\sigma_{1\text{ M KCl}}$). Column ΔG / ($\sigma \times d_{\text{DNA}}$) ≤ 1 weighs ΔG by electrolyte conductivity and DNA diameter size (2.2 and 1.1 nm, respectively, for dsDNA and ssDNA). Gray rows correspond to measurements made with ssDNA. The yellow row indicates the highest ΔG obtained in this work. (†) Indicates when values of σ were not quoted in the reference; we assumed values of 7.0, 7.8 and 10.8 S m^{-1} for 1 M solutions of Li, Na and K chloride at 23°C, respectively.[39] Temperatures at which conductivities were measured are indicated for temperatures other than room temperature (23°C). (*) Indicates that values of nanopore diameter d or membrane thickness t quoted in the reference were obtained indirectly from a fit to a model of nanopore conductance.

ASSOCIATED CONTENT

Supporting Information. Details explaining the effective thickness calculation, molecular dynamics parameters, statistical analysis of translocations data, and analysis of electrolyte conductivity are provided. An additional ionic current trace showing translocations of 400 bp dsDNA at 500 mV is given together with the complete datasets for all nanopores analyzed in this work. This material is available free of charge *via* the Internet at http://pubs.acs.org.

AUTHOR INFORMATION

Corresponding Author

* E-mail: (J.A.R.-M.) rjulio@sas.upenn.edu

* E-mail: (M.D.) drndic@physics.upenn.edu

Author Contributions

⊥J.A.R.-M. and M.P contributed equally to this work. J.A.R.-M and M.D. designed the experiments; J.A.R.-M designed the thinning method, fabricated nanopores and analyzed the STEM data; M.P. performed translocation measurements and analyzed the ionic current data; A.N. and V.M. performed the computational simulations and analyzed the molecular dynamics trajectories. All authors contributed in the discussion and writing of the manuscript.

Notes

The authors declare no competing financial interest.

ACKNOWLEDGMENT

This work was supported by NIH Grant R21HG004767 and R01HG006879, and by the Nano/Bio Interface Center through the National Science Foundation NSEC DMR08-32802. We gratefully acknowledge use of the TEM in the NSF-MRSEC electron microscopy facility at the University of Pennsylvania. M.P. acknowledges funding from the NSF-IGERT program (Grant DGE-0221664). Work at Rensselaer was sponsored by the Office of Naval Research and all computations were performed at the Center of Computational Innovations (CCI) at Rensselaer Polytechnic Institute.

REFERENCES

(1) Dekker, C. Solid-State Nanopores. *Nat. Nanotechnol.* **2007,** *2*, 209-215.

(2) Ivanov, A. P.; Instuli, E.; McGilvery, C. M.; Baldwin, G.; McComb, D. W.; Albrecht, T.; Edel, J. B. DNA Tunneling Detector Embedded in a Nanopore. *Nano Lett.* **2010,** *11*, 279-285.

(3) Xie, P.; Xiong, Q.; Fang, Y.; Qing, Q.; Lieber, C. M. Local Electrical Potential Detection of DNA by Nanowire-Nanopore Sensors. *Nat. Nanotechnol.* **2012,** *7*, 119-125.

(4) Puster, M.; Rodríguez-Manzo, J. A.; Balan, A.; Drndić, M. Toward Sensitive Graphene Nanoribbon–Nanopore Devices by Preventing Electron Beam-Induced Damage. *ACS Nano* **2013,** *7*, 11283-11289.

(5) Traversi, F.; Raillon, C.; Benameur, S. M.; Liu, K.; Khlybov, S.; Tosun, M.; Krasnozhon, D.; Kis, A.; Radenovic, A. Detecting the Translocation of DNA Through a Nanopore Using Graphene Nanoribbons. *Nat Nanotechnol.* **2013,** *9*, 939-945.

(6) Larkin, J.; Foquet, M.; Turner, S. W.; Korlach, J.; Wanunu, M. Reversible Positioning of Single Molecules inside Zero-Mode Waveguides. *Nano Lett.* **2014,** *14*, 6023-6029.

(7) Tabard-Cossa, V.; Trivedi, D.; Wiggin, M.; Jetha, N. N.; Marziali, A. Noise Analysis and Reduction in Solid-State Nanopores. *Nanotechnol.* **2007,** *18*, 305505.

(8) Smeets, R. M. M.; Keyser, U. F.; Dekker, N. H.; Dekker, C. Noise in Solid-State Nanopores. *Proc. Natl. Acad. Sci. U. S. A.* **2008,** *105*, 417-421.

(9) Rosenstein, J. K.; Wanunu, M.; Merchant, C. A.; Drndić, M.; Shepard, K. L. Integrated Nanopore Sensing Platform with Sub-Microsecond Temporal Resolution. *Nat. Methods* **2012,** *9*, 487-492.

(10) Balan, A.; Machielse, B.; Niedzwiecki, D.; Lin, J.; Ong, P.; Engelke, R.; Shepard, K. L.; Drndić, M. Improving Signal-to-Noise Performance for DNA Translocation in Solid-State Nanopores at MHz Bandwidths. *Nano Lett.* **2014,** *14*, 7215-7220.

(11) Manrao, E. A.; Derrington, I. M.; Laszlo, A. H.; Langford, K. W.; Hopper, M. K.; Gillgren, N.; Pavlenok, M.; Niederweis, M.; Gundlach, J. H. Reading DNA at Single-Nucleotide Resolution with a Mutant MspA Nanopore and phi29 DNA Polymerase. *Nat. Biotechnol.* **2012,** *30*, 349-353.

(12) Hall, J. E. Access Resistance of a Small Circular Pore. *J. Gen. Physiol.* **1975,** *66*, 531-532.

(13) Kowalczyk, S. W.; Grosberg, A. Y.; Rabin, Y.; Dekker, C. Modeling the Conductance and DNA Blockade of Solid-State Nanopores. *Nanotechnol.* **2011,** *22*, 315101.

(14) Wanunu, M.; Dadosh, T.; Ray, V.; Jin, J.; McReynolds, L.; Drndić, M. Rapid Electronic Detection of Probe-Specific MicroRNAs Using Thin Nanopore Sensors. *Nat. Nanotechnol.* **2010,** *5*, 807.

(15) Venta, K.; Shemer, G.; Puster, M.; Rodríguez-Manzo, J. A.; Balan, A.; Rosenstein, J. K.; Shepard, K.; Drndić, M. Differentiation of Short, Single-Stranded DNA Homopolymers in Solid-State Nanopores. *ACS Nano* **2013,** *7*, 4629-4636.

(16) Hall, A. R. *In Situ* Thickness Assessment During Ion Milling of a Free-Standing Membrane Using Transmission Helium Ion Microscopy. *Microsc. Microanal.* **2013,** *19*, 740-744.

(17) Merchant, C. A.; Healy, K; Wanunu, M; Vishva, R; Peterman, N; Bartel, J; Fischbein, M. D.; Venta, K.; Luo, Z.; Johnson, A. T. C.; et al. DNA Translocation through Graphene Nanopores. *Nano Lett.* **2010,** *10*, 2915.

(18) Schneider, G. F.; Kowalczyk, S. W.; Calado, V. E.; Pandraud, G.; Zandbergen, H. W.; Vandersypen, L. M. K.; Dekker, C. DNA Translocation through Graphene Nanopores. *Nano Lett.* **2010,** *10*, 3163-3167.

(19) Garaj, S.; Hubbard, W.; Reina, A.; Kong, J.; Branton, D.; Golovchenko, J. A. Graphene as a Subnanometre Trans-Electrode Membrane. *Nature* **2010,** *467*, 190-193.

(20) Garaj, S.; Liu, S.; Golovchenko, J. A.; Branton, D. Molecule-Hugging Graphene Nanopores. *Proc. Natl. Acad. Sci. U. S. A.* **2013,** *110*, 12192-12196.

(21) Liu, S.; Lu, B.; Zhao, Q.; Li, J.; Gao, T.; Chen, Y.; Zhang, Y.; Liu, Z.; Fan, Z.; Yang, F.; et al. Boron Nitride Nanopores: Highly Sensitive DNA Single-Molecule Detectors. *Adv. Mater.* **2013,** *25*, 4549-4554.

(22) Zhou, Z.; Hu, Y.; Wang, H.; Xu, Z.; Wang, W.; Bai, X.; Shan, X.; Lu, X. DNA Translocation through Hydrophilic Nanopore in Hexagonal Boron Nitride. *Sci. Rep.* **2013,** *3*.

(23) Larkin, J.; Henley, R.; Bell, D. C.; Cohen-Karni, T.; Rosenstein, J. K.; Wanunu, M. Slow DNA Transport through Nanopores in Hafnium Oxide Membranes. *ACS Nano* **2013,** *7*, 10121-10128.

(24) Shim, J.; Rivera, J. A.; Bashir, R. Electron Beam Induced Local Crystallization of HfO_2 Nanopores for Biosensing Applications. *Nanoscale* **2013,** *5*, 10887-10893.

(25) Liu, K.; Feng, J.; Kis, A.; Radenovic, A. Atomically Thin Molybdenum Disulfide Nanopores with High Sensitivity for DNA Translocation. *ACS Nano* **2014,** *8*, 2504-2511.

(26) Egerton, R. F.; Li, P.; Malac, M. Radiation Damage in the TEM and SEM. *Micron* **2004,** *35*, 399.

(27) Wu, M.-Y.; Krapf, D.; Zandbergen, M.; Zandbergen, H.; Batson, P. E. Formation of Nanopores in a SiN/SiO_2 Membrane with an Electron Beam. *Appl. Phys. Lett.* **2005,** *87*, 113106.

(28) Howitt, D. G.; Chen, S. J.; Gierhart, B. C.; Smith, R. L.; Collins, S. D. The Electron Beam Hole Drilling of Silicon Nitride Thin Films. *J. Appl. Phys.* **2008,** *103*, 024310.

(29) Carlsen, A. T.; Zahid, O. K.; Ruzicka, J.; Taylor, E. W.; Hall, A. R. Interpreting the Conductance Blockades of DNA Translocations through Solid-State Nanopores. *ACS Nano* **2014,** *8*, 4754-4760.

(30) Yanagi, I.; Akahori, R.; Hatano, T.; Takeda, K.-i. Fabricating Nanopores with Diameters of Sub-1 nm to 3 nm Using Multilevel Pulse-Voltage Injection. *Sci. Rep.* **2014,** *4*, 5000.

(31) Egerton, R. F. *Electron Energy-Loss* Spectroscopy *in the Electron Microscope*. Second ed.; Plenum Press: New York, 1996.

(32) Briggs, K.; Kwok, H.; Tabard-Cossa, V. Automated Fabrication of 2-nm Solid-State Nanopores for Nucleic Acid Analysis. *Small* **2014,** *10*, 2077-2086.

(33) Cueva, P.; Hovden, R.; Mundy, J. A.; Xin, H. L.; Muller, D. A. Data Processing for Atomic Resolution Electron Energy Loss Spectroscopy. *Microsc. Microanal.* **2012,** *18*, 667-675.

(34) Plimpton, S. Fast Parallel Algorithms for Short-Range Molecular Dynamics. *J. Comput. Phys.* **1995,** *117*, 1-19.

(35) Ishimaru, M.; Munetoh, S.; Motooka, T. Generation of Amorphous Silicon Structures by Rapid Quenching: A Molecular-Dynamics Study. *Phys. Rev. B* **1997,** *56*, 15133-15138.

(36) Stillinger, F. H.; Weber, T. A. Computer Simulation of Local Order in Condensed Phases of Silicon. *Phys. Rev. B* **1985,** *31*, 5262-5271.

(37) Djordjević, B. R.; Thorpe, M. F.; Wooten, F. Computer Model of Tetrahedral Amorphous Diamond. *Phys. Rev. B* **1995,** *52*, 5685-5689.

(38) Krzeminski, C.; Brulin, Q.; Cuny, V.; Lecat, E.; Lampin, E.; Cleri, F. Molecular Dynamics Simulation of the Recrystallization of Amorphous Si layers: Comprehensive Study of the Dependence of the Recrystallization Velocity on the Interatomic Potential. *J. Appl. Phys.* **2007,** *101*, 123506.

(39) *CRC Handbook of Chemistry and Physics,*79th ed.; Lide, D. R., Ed.; CRC Press: Boca Raton, 1998.

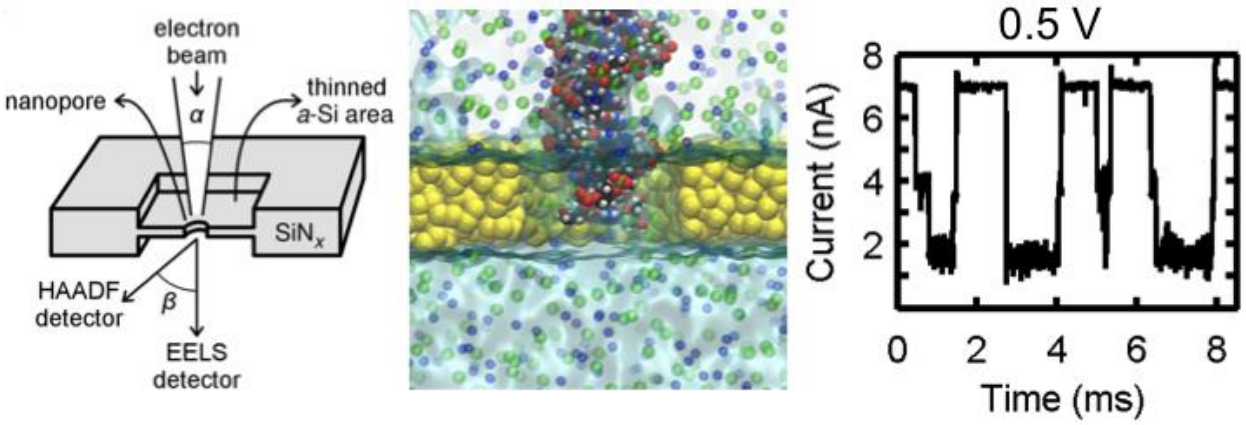

Schematic of membrane thinning with the electron beam, molecular dynamics model of the DNA and the *a*-Si nanopore, and the measured translocation signals.